Radiation patterns from vortex-antivortex annihilation

Matthew W. Hecht and Thomas A. DeGrand
Physics Department, University of Colorado, Boulder, Colorado 80309
(Received 8 January 1990)

We simulate vortex-antivortex annihilation in (2+1)-dimensional O(2) scalar field theory, under a variety of initial conditions. In all cases the energy density of Goldstone-boson radiation shows a $\sin^2\alpha$ dependence on the angle α from the final approach due to emission from linear acceleration during the approach and from the overlap of the vortex cores. In collisions at a nonzero impact parameter, there is additional radiation due to circular acceleration. We explore the usefulness of an electromagnetic analogy which uses the vortex world lines as dynamic variables. Our calculations are relevant to the annihilation of antiparallel cosmic strings.

I. INTRODUCTION

One-dimensional topological defects (strings) may exist in field theories which possess global or local symmetries. If field theories which can support string degrees of freedom are relevant for the description of the early Universe, cosmic strings could have arisen as the Universe cooled through a phase transition via the Kibble[1] mechanism, and have been suggested to explain a variety of cosmological features.[2] Oscillating string loops may have been the seeds of the large-scale structure which is seen in the Universe today.[3,4] Long strings which cross the horizon could have survived until the present age, existing as highly massive relics of a time when the Universe was incredibly hot and dense.

In studies of string dynamics in the early Universe the most important problem has been the elucidation of string intercommutation. One is interested in finding the distribution of string matter as a function of time. Among others, Shellard has investigated the dynamics of global cosmic strings,[5] while Matzner,[6] and Moriarty, Myers, and Rebbi[7] have considered the scattering of cosmic strings possessing a local gauge invariance. Albrecht and Turok[8] and Bennett and Bouchet[9] have recently studied the evolution of string networks in approaches which deal directly with the string world lines rather than with an underlying field theory.

In this paper we focus on the physics of annihilation of topological degrees of freedom in classical O(2) scalar field theory. Because the number of possible degrees of freedom which can be varied for systems in three spatial dimensions is very large, we have elected to work in two spatial dimensions. Thus, the topological defects are point defects, vortices, and antivortices. In cosmic-string language, this paper is concerned with the Goldstone-boson-radiation pattern produced when a pair of antiparallel cosmic strings annihilate. We believe our investigations have an interest beyond early Universe studies. Our results have applications to other physical systems, such as two-dimensional films of liquid crystals,[10] or generally, to the kinetics of X-Y models. (Vortices in liquid helium are more complicated.[11]) Many of the gross features we observe have been previously reported but we believe that a number of our observations are new.

Finally, it has been known for some time that an analog Lagrangian can be derived for complex scalar field theories which involves only point interactions.[12,13] In two spatial dimensions this point interaction takes on the familiar form of electromagnetism. We find that many of the qualitative features of vortex-antivortex annihilation are reproduced by a model containing electromagnetic point sources. However, the electrodynamic analogy appears not to be useful for detailed studies of annihilation dynamics.

Numerical simulation of vortex annihilation in a complex scalar field is treated in Sec. II. Section III covers the analogous model, with point electromagnetic particles replacing the vortices. The last section contains our conclusions. The derivation of the equivalence of the effective, electromagnetic Lagrangian to the Lagrangian for the complex scalar field is outlined in the Appendix.

II. VORTEX-ANTIVORTEX ANNIHILATION IN A COMPLEX SCALAR FIELD

A. Field variables

We will study the complex scalar field theory whose Lagrange density is

$$L=\tfrac{1}{2}(\partial_\mu\Phi^*)(\partial^\mu\Phi)-\frac{\lambda}{4}(\Phi^*\Phi-\eta^2)^2 . \tag{2.1}$$

The two components of Φ can be taken to be ϕ_1 and ϕ_2, or ρ and θ, where

$$\begin{aligned}\Phi(x,y,t)&=\phi_1(x,y,t)+i\phi_2(x,y,t)\\&=\rho(x,y,t)e^{i\theta(x,y,t)} .\end{aligned} \tag{2.2}$$

Three types of excitations occur. Two are local: a massless Goldstone excitation corresponding roughly to excitations of θ modes; and a Higgs boson or massive mode, corresponding roughly to excitations of ρ modes. Additionally, the field supports vortex and antivortex excitations.

The vorticity of any region may be defined by

$$\oint \phi^i dx^i = 2\pi\eta \ , \tag{2.3}$$

where η is the vorticity, taking on values $\eta = 0, \pm 1, \pm 2, \ldots$. Objects of vorticity of magnitude greater than one may be constructed, but are known to be unstable against decay into multiple $|\eta| = 1$ objects,[5] and are not considered in this paper.

A simple expression for the Φ field which describes an isolated vortex at the origin of coordinate space is

$$\Phi_v = \rho(x,y) e^{i\theta(x,y)} = \rho(x,y) \frac{x+iy}{r} \ , \tag{2.4}$$

where the phase is now given by the particular solution $\tan\theta(x,y) = y/x$. An isolated antivortex is described by the complex conjugate of (2.4). The coordinates may be boosted to give Φ for a moving vortex.

The Euler-Lagrange equation in the static limit,

$$\rho'' + \frac{\rho'}{r} - \frac{\rho}{r^2} - \lambda\rho(\rho^2 - \eta^2) = 0 \ , \tag{2.5}$$

can be integrated to give $\rho(r)$. The choice of coupling and vacuum expectation value defines the core radius r_c, below which ρ deviates significantly from η. In terms of the vacuum expectation value and the coupling.

$$r_c \approx \frac{1}{\eta} \left[\frac{2}{\lambda} \right]^{1/2} \ . \tag{2.6}$$

We will measure all distances and times in units of $1/\eta\sqrt{1/\lambda}$, and energies in units of $\eta\sqrt{\lambda}$.

For $r \ll r_c$, $\rho(r)$ is approximately linear in r, while for $r \gg r_c$ the solution has the form $\rho(r) = \eta - O(r^{-1})$. In the intermediate region, the differential equation can be integrated numerically. A graph of $\rho(r)$ is given by Shellard.[5]

B. The numerical simulation

We have carried out an extensive program of numerical simulations of vortex-antivortex annihilation. The simulation is begun at $t = 0$ by specifying a set of values of field variables Φ and time derivatives corresponding to locating a vortex and an antivortex at some initial coordinates with some initial velocities. The pair attract each other through a logarithmic potential. We evolve the microscopic equations of motion forward in time, through annihilation, until the radiation pattern is seen. In order to perform the simulation, the continuum equations of motion are discretized in space, with a lattice spacing a. The resulting pair of simultaneous, first-order differential equations are

$$\frac{dP_\beta(\mathbf{r})}{dt} = -\lambda\phi_\beta(\mathbf{r})[\phi_\alpha(\mathbf{r})\phi_\alpha(\mathbf{r}) - \eta^2] - \frac{1}{a^2} \sum_{nn} [\phi_\beta(\mathbf{r}) - \phi_\beta(nn)] \ , \tag{2.7}$$

$$\frac{d\phi_\beta(\mathbf{r})}{dt} = P_\beta(\mathbf{r}) \ , \tag{2.8}$$

where the sum on nn runs over nearest neighbors. Our simulations are performed at the particular choice of coupling and vacuum expectation value $\lambda = 1$ and $\eta = 1$, which sets the core radius at about $\sqrt{2}$. The time evolution of the system is integrated using a leapfrog algorithm, which is accurate to second order in the time step. We use steps of $\Delta t = 0.1$ and $a = 0.5$. For vortex velocities less than $0.9c$ we do not see lattice effects in our simulations with these parameters.

Typical simulation areas are squares of length $L = 60$ on a side (120^2 lattice sites). We use open boundary conditions. To minimize reflections, a damping term is added to Eq. (2.7), for all sites which lie on the boundary. The extra term is proportional to the momentum; the constant of proportionality is chosen to minimize the reflected energy.

To set a vortex-antivortex pair down on a lattice at positions $\mathbf{x}_{v_0}$ and $\mathbf{x}_{\bar{v}_0}$, we take Φ to be the product of the solutions for an isolated vortex and for an isolated antivortex, as

$$\Phi = \Phi_v(x_{v_0}) \Phi_{\bar{v}}(x_{\bar{v}_0}) \ . \tag{2.9}$$

If the initial velocity is nonzero, then $P(t=0) = (d\Phi/dt)_{t=0}$. We replace the time derivative by a finite difference over a small time step (using $\Delta t = 0.05$), which is a reasonably stable method of initializing the velocity.

C. Features at zero impact parameter

We begin by showing, in Fig. 1, a series of plots of the energy density at several time steps, from a simple initial configuration with the vortex and antivortex separated 20 spatial units apart with zero velocity. The energy density is symmetric with respect to reflections across either axis, or across the origin, so in this figure we show only the $x > 0, y > 0$ quadrant. In the final snapshot, one can see that the energy has been radiated primarily in a direction transverse to the path of approach, at 90°; in fact, there are nodes at 0° and 180°. A more subtle feature of the pattern is that there is a radial node as well, separating the major, inner peak in the energy density from a smaller, outer peak. The inner peak carries off the energy from the annihilation, while the outer peak was radiated during the approach. The amount of energy within the inner and outer peaks is nearly equal for this set of initial conditions [plotted in Fig. 1(a)].

At the late stages of a simulation, the energy is almost entirely in the θ modes, so that the Lagrangian, can be reduced to $L \approx \frac{1}{2}\partial_\mu\Phi^*\partial^\mu\Phi$. This leads to an energy density $u \approx \frac{1}{2}\eta^2(\partial^\mu\theta)^2$. When the final plot of Fig. 1 was taken, 95% of the energy was in θ modes.

Figure 2 shows a phase plot of the same radiated wave as Fig. 1. The derivatives of the phase go to zero at the peak of the outgoing ripple; this is where the radial node occurs in the energy density. The electromagnetic analog to the Φ problem, which is developed in the next section, casts additional light upon the radial structure of the Goldstone-boson radiation.

We performed a partial-wave analysis to probe the angular structure. We decompose the amplitude $\partial^\mu\Phi$ into

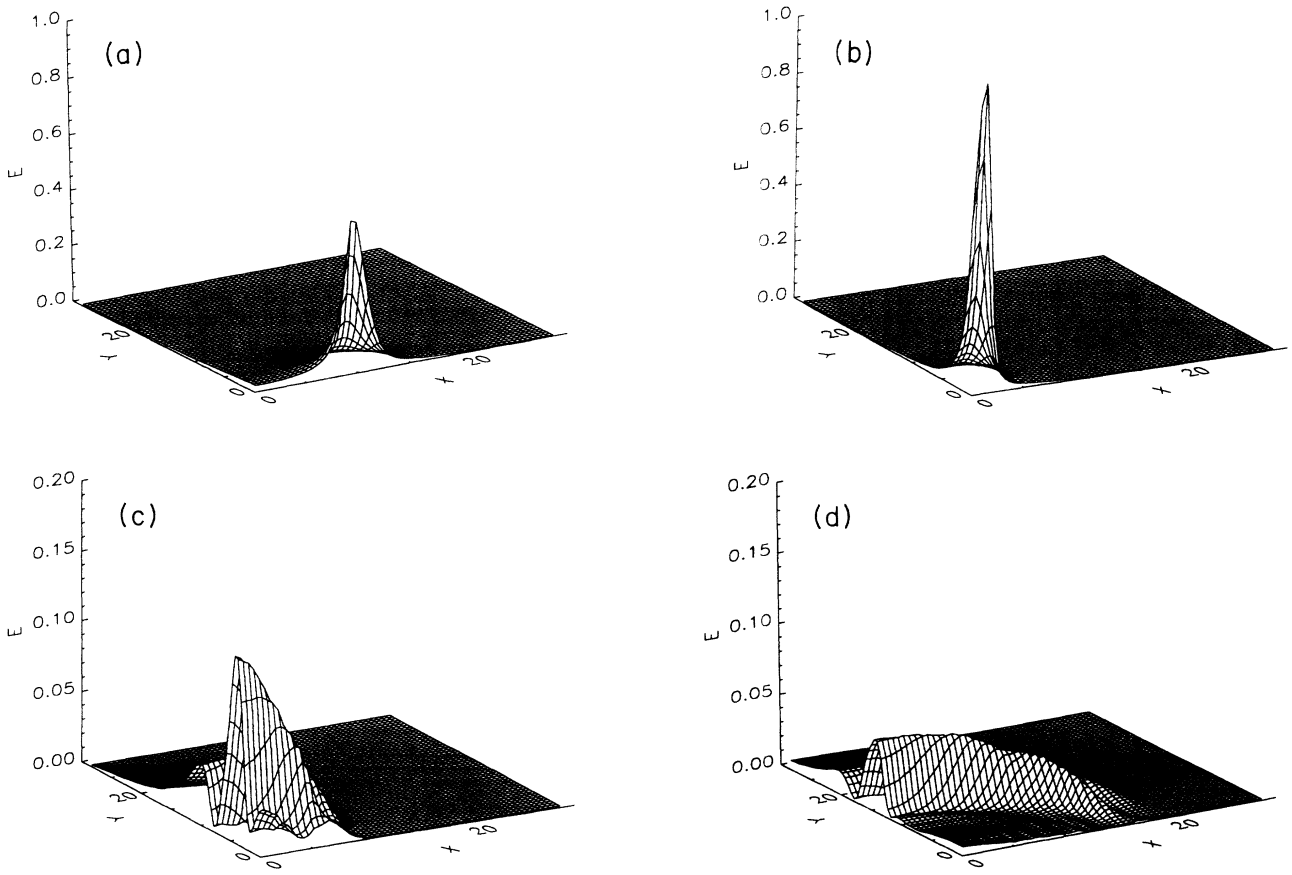

FIG. 1. Annihilation from zero initial velocity at an initial separation of 20 spatial units: (a) at $t=0$; (b) at annihilation, $t=20$; (c) at $t=30$; and (d) at $t=40$. The energy density is symmetric with respect to reflections across either axis, or across the origin, so we show only the $x>0, y>0$ quadrant.

sine and cosine terms, integrating out the radial dependence, to obtain the angular spectrum. The radiation is emitted almost entirely in a dipole pattern, as can be seen in Fig. 3.

We ran simulations at a range of energies. As the initial velocity is increased a threshold is encountered,

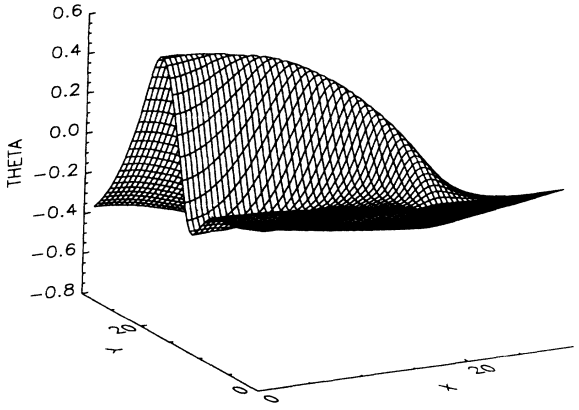

FIG. 2. Phase of the complex field. This snapshot corresponds to Fig. 1(d).

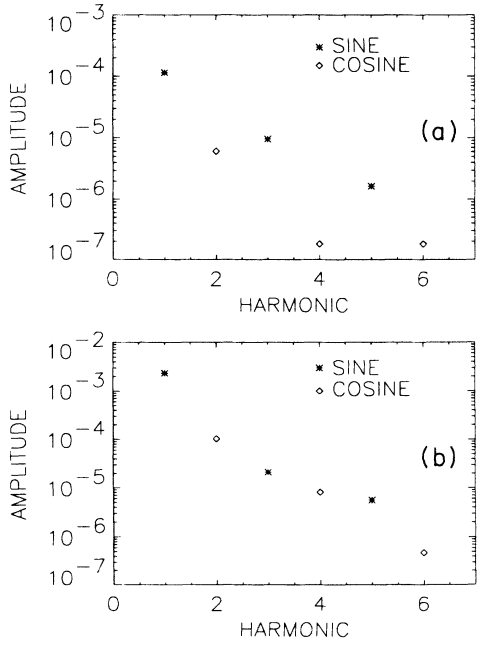

FIG. 3. Results of partial-wave analysis on the radiation fields: (a) zero initial velocity; and (b) initial velocity of 0.5. Initial separation of 20 spatial units

above which the pair emerge some short distance and then crash back into extinction (this threshold was first noted by Shellard, in Ref. 5). For the particular lattice size, initial positions, and field parameters which we use, the threshold is at an energy of about 21 units, corresponding to an initial velocity of 0.2 with an initial separation of 20 spatial units.

The path of a vortex is monitored in a coarse manner by evaluating the change in the phase of the field around a plaquette; we implement fine tracking by assuming a linear zero in the ρ field. The particle world lines are displayed in Fig. 4 for a variety of initial energies above the inelastic threshold.

In these collisions the vortex and antivortex pass through each other (scatter at 0°). This would not be too remarkable (after all, the outer regions of the colliding pair do not know that the annihilation has occurred, and their inertia can cause the v-$\bar{v}$ pair to reform after annihilation), were it not for the fact that local strings behave differently. Moriarty, Myers, and Rebbi[7] report 180°, inelastic scattering of local v-$\bar{v}$ pairs.

While the pair scatter at 0°, they emerge with their phases rotated by 180°. At large distances the field points in one predominant direction. If that orientation is in the positive $\hat{x}$ direction, and the vortex, is placed along the negative x axis, then it must be that, for points close to the vortex, the field points inward. After the pair pass through one another the field must point out from the vortex, since the field at large distances maintains the same orientation. A similar analysis of the field around the antivortex leads to the conclusion that the pair must emerge phase shifted by 180°, as we observe.

A series of energy plots from a representative run at a higher energy appears in Fig. 5. Quadruple rings are visible in the final picture; the outermost rings from the approach, the next from passing through one another, and the inner two rings from the final approach and then annihilation. Again the radiation pattern from both rings shows a dipole pattern with little discernible energy variation.

The maximum separation that the pair reach, as a function of energy, appears in Fig. 6. If the fraction of energy lost was independent of initial energy, we would see a maximum separation with an exponential dependence on the energy, due to the logarithmic potential between the v-$\bar{v}$ pair; a much slower rise with energy is observed. Clearly the fraction of the initial energy, which is lost in the approach and pass through, rises with energy.

It is less clear whether or not a resonant state is formed. Tracking the pair is difficult when they are very close; the data is consistent with either the formation of a resonant state whose lifetime is roughly independent of the initial energy, or with the lack of a resonance but with very slow motion immediately after the pair pass through each other. Resolution of this issue requires a much finer lattice spacing and more computer capacity than we currently possess.

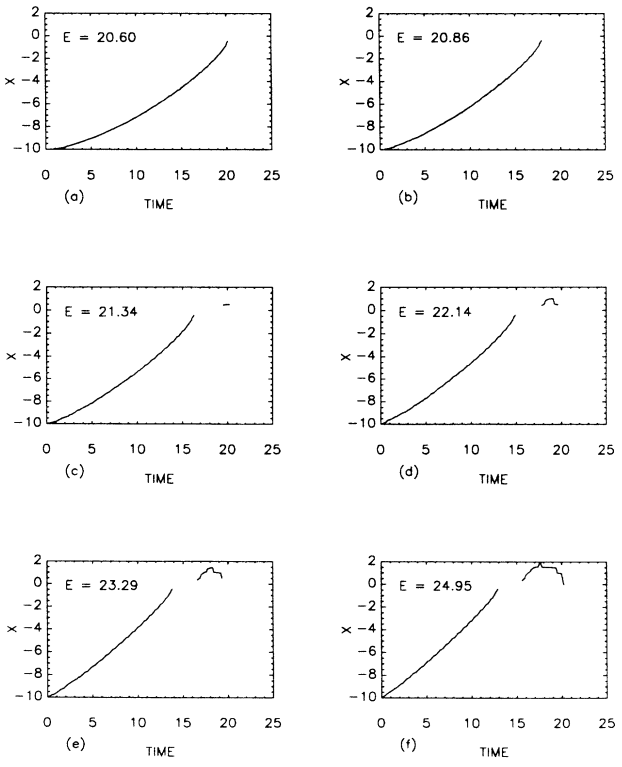

FIG. 4. Vortex world lines for six different initial energies. The data is consistent with either the formation of a resonant state whose lifetime is roughly independent of the initial energy, or with the lack of a resonance but with very slow, low-energy motion after passing through. Initial velocities were 0.0, 0.1, . . . , 0.5, with an initial separation of 20 units.

D. Features at nonzero impact parameter

We have also carried out vortex-antivortex collisions in which the pair is set down with some initial velocity in the x direction, at some nonzero impact parameter. Simulations at several different impact parameters are recorded in Fig. 7. For these simulations the energy is symmetric with respect to reflection across the origin, so we show the $y > 0$ half of the pattern only. Some of the qualitative features of the annihilation pattern resemble the zero-impact-parameter case, but overall the pattern is much richer. Again there is a radial node in the energy density. The energy inside the node was radiated during the annihilation, and looks much like the dipole radiation from zero-impact-parameter runs. The final approach of the v-$\bar{v}$ pair lies at some angle to the x axis, as illustrated in Fig. 8. The orientation of the dipole radiation clearly is rotated by this same angle.

Whereas the energy contained in the inner wave is weakly dependent on impact parameter, the outer wave is strongly dependent on it. With rising impact parameter, the outer wave becomes more substantial, as the vortices lose energy and angular momentum. The outer wave also shows more structure. In the head-on collisions, the vortices only undergo linear acceleration. In the more general case of nonzero impact parameter, the motion at any time can be decomposed into a linear and a circular component. While the energy loss due to linear acceleration is radiated most strongly transverse to the motion, that

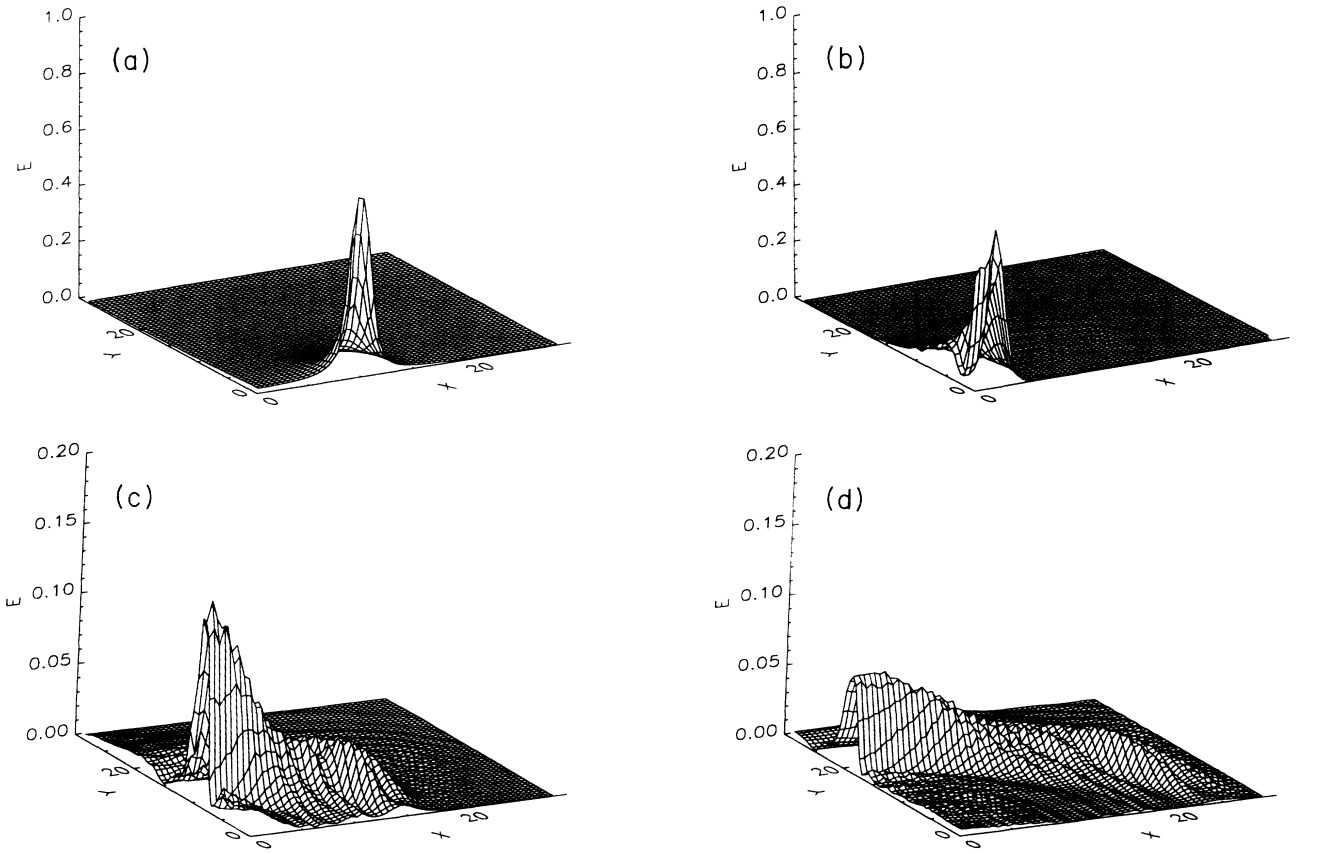

FIG. 5. Annihilation from an initial velocity of 0.5, initial separation of 20 spatial units: (a) at $t=0$; (b) pair has passed through one another at $t=17.5$; (c) radiated wave at $t=30$; and (d) at $t=40$. The energy density is symmetric with respect to reflections across either axis, or across the origin, so we show only the $x>0, y>0$ quadrant.

due to circular acceleration is radiated primarily at a tangent to the path. Both mechanisms of energy loss are identifiable in the plots of Fig. 7, where A labels the wave from annihilation, B labels the wave radiated due to linear acceleration, and C labels the wave from circular acceleration.

If the annihilation were from zero impact parameter, one would expect to see a node in the angular momentum at 90° to the line along which the approach took place, where the energy flow is purely radial. If the angular momentum at angle $90°-\delta$ is positive, then the symmetry of the problem requires that the angular momentum at angle $90°+\delta$ be negative. In addition to this symmetry about the 90° line, the angular momentum will vary in intensity and sign with radial distance, as the field oscillates with the passing of the radiated wave.

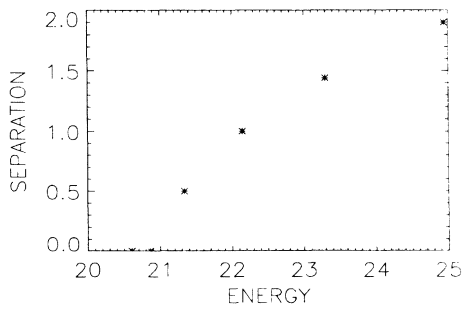

FIG. 6. Maximum v-$\bar{v}$ separation after passing through one another for six different sets of initial conditions.

The angular momentum density for a typical set of initial conditions at nonzero impact parameter is shown in Fig. 9. The reduced symmetry of the initial configuration results in a more complex angular momentum pattern, yet the reader may identify both the node in the angular momentum at the radial peak of the radiated wave [as seen in the energy plot of Fig. 7(b)], indicating a point which lies at 90° to the final line of approach of the v-$\bar{v}$ pair, as well as the variation in intensity and sign with radial distance which reflects the oscillation of the field.

III. THE ELECTROMAGNETIC ANALOGY

A. Equivalence to the electromagnetic Lagrangian

The interaction of global cosmic strings with the Goldstone-boson field is hard to analyze. However, the string core size is typically small in comparison to the separation between strings, and a number of authors have shown that this topological problem can be translated to

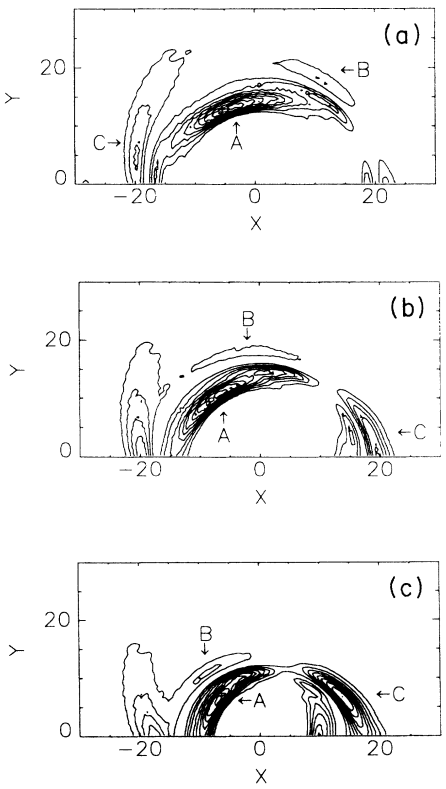

FIG. 7. Energy contours at $t=35$, for runs at nonzero impact parameter, all with initial velocities of 0.5. (a) Initial positions of $\mathbf{x}_v=(-10,-3)$, $\mathbf{x}_{\bar{v}}=(10,3)$; (b) initial positions of $\mathbf{x}_v=(-10,-6)$, $\mathbf{x}_{\bar{v}}=(10,6)$; and (c) initial positions of $\mathbf{x}_v=(-10,-9)$, $\mathbf{x}_{\bar{v}}=(10,9)$. A labels wave from annihilation; B from linear acceleration; C from circular acceleration. Contours are drawn at energy levels of 0.01,0.02, ... The energy density is symmetric with respect to reflection across the origin, so we show the $y>0$ half of the antennae pattern only.

one of a string source interacting with an antisymmetric tensor field produced by other strings.[12,13,14] The interaction of the string with the Goldstone-boson field radiated by other strings reduces to a problem of local interactions.

It is straightforward to reduce the string calculations,

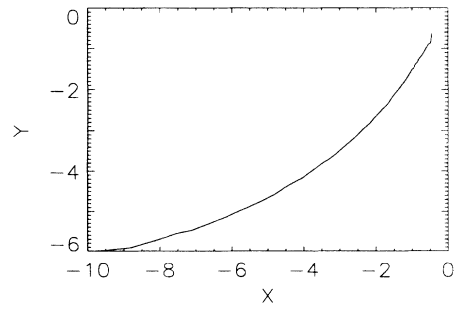

FIG. 8. Vortex path. Initial velocity was 0.5, initial positions of $\mathbf{x}_v=(-10,-6)$, $\mathbf{x}_{\bar{v}}=(10,6)$. See Fig. 7(b) for corresponding energy plot.

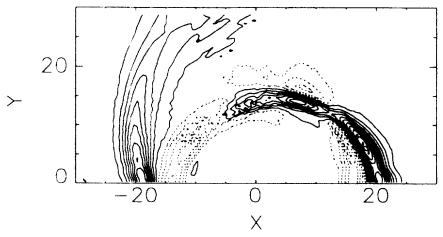

FIG. 9. Angular momentum at $t=35$. Initial velocity of 0.5, from initial positions of $\mathbf{x}_v=(-10,-6)$, $\mathbf{x}_{\bar{v}}=(10,6)$ which corresponds to Fig. 7(b). Solid lines are contours at 0.0125,0.0375, ...; dotted lines at −0.0125, −0.0375, ...

done in three spatial dimensions, down to the two-dimensional case. In the (2+1)-dimensional case the antisymmetric tensor becomes the electromagnetic field tensor, and the problem of the vortex coupled to Goldstone bosons is found to be equivalent to that of a point charge interacting locally with an electromagnetic field. We present a derivation of this equivalence, which parallels that of Vilenkin and Vachaspati,[12] in the Appendix. The result is that

$$L_{\text{eff}}=-\frac{1}{16\pi}F_{\alpha\beta}F^{\alpha\beta}-J_\alpha A^\alpha \tag{3.1}$$

where

$$J_\alpha(x)=g\int V_\alpha(\mathbf{x}')\delta^{(3)}(\mathbf{x}-\mathbf{x}')dx'_0 \tag{3.2}$$

is the current of a pointlike vortex core (V_α is its velocity three-vector). The coupling is proportional to the vacuum expectation value, as

$$g=\sqrt{\pi}\eta\ , \tag{3.3}$$

and the vector potential is related to the phase of the Φ field by

$$2\sqrt{\pi}\eta\partial_\mu\theta=\tfrac{1}{2}\epsilon_{\mu\alpha\beta}F^{\alpha\beta}\ . \tag{3.4}$$

B. Applying the electromagnetic analogy

The tool with which to do electrodynamics is the (2+1)-dimensional Green's function

$$G(r,t;0,0)=\frac{2}{\sqrt{t^2-r^2}}\Theta(t-|r|)\ . \tag{3.5}$$

Calculations in (2+1) dimensions are more difficult than in (3+1), because the Green's function is dispersive. The physical basis for this dispersion is easy to understand if one remembers that the (2+1)-dimensional case can be thought of as (3+1)-dimensional, with z independence. This is the physics of long straight charged rods. When the rod is accelerated, an observer first sees the effect due to the closest point on the rod (the θ function turns on), but then sees a continuing signal which grows ever fainter, emitted from segments of the rod which are further and further distant.

As always, the vector potential is calculated by integrating over the source, weighted by the Green's function:

$$A_\mu(r,t)=\int G(r,t;r',t')J_\mu(r',t')d^3x' \ . \tag{3.6}$$

Closed forms for the Liénard-Wiechert potentials do not exist, except for particularly simple source functions. For instance, for simple harmonic motion the **A** field is

$$\mathbf{A}(r,t)\propto\hat{\mathbf{x}}\sin(\omega t)H_0(kr)\propto\hat{\mathbf{x}}\sin(\omega t)\frac{e^{ikr}}{\sqrt{kr}} \ , \tag{3.7}$$

which results in a dipolar radiation pattern. The dipole pattern of simple harmonic string motion was first given by Davis[15] without using the language of the antisymmetric tensor field. Other examples are described by Davis and Shellard.[16] In more complicated cases such as ours, the potentials can be found numerically.

C. Calculating the energy density numerically

We are interested in computing the energy antenna pattern in head-on vortex-antivortex annihilation using the electromagnetic analogy. Any source function may be used in the calculation of the vector potential. In principle, one can calculate an analytic form for the vortex path by integrating the equations of motion for a vortex in the potential of another vortex. In fact the motion is relativistic, and the calculation requires the inclusion of radiative back reactions since we know that the vortex radiates a large fraction of its energy during infall. Dabholkar and Qaushnock[17] have calculated the evolution of loops of global string for which the loop radius is much larger than the string core radius, including the effects of radiative back reactions in their treatment. We short cut this tedious process, using the vortex world line as the source (which automatically includes the back reaction), as recorded in simulations using the original Lagrangian.

There is one region which poses a dilemma, and that is where the cores of the vortices overlap. Classical field theories do not accommodate particle annihilation. Furthermore, the derivation of the equivalence of the Φ and electromagnetic Lagrangians becomes unsound as the pair overlaps, at annihilation. This happens to be the region where most of the Goldstone-boson radiation is produced.

One apparent solution is to extrapolate the motion of the vortex and antivortex assuming a linearly increasing velocity over the final distance and cutting off the currents at the annihilation point. There is a serious difficulty inherent to this approach, which is that the source vanishes in an instant, which neither reflects the more gradual dissolution of the vortex and antivortex, nor does it lead to a well-behaved vector potential. (Discontinuous derivatives in the current create cusps in the radiated energy density.) A better solution, which we pursued, is to mimic the final throes of annihilation by linearly extrapolating the velocity to zero as the vortex cores overlap. The test of the method will be made by comparison to the Φ data.

In passing, we note that the integrand from which the vector potential is calculated contains a square-root singularity. It is treated with appropriate care.

D. Qualitative features of the radiation pattern from the electromagnetic analogy

Much of the behavior of the energy density can be found without doing any calculations. Let us assume we are modeling a head-on collision, so the motion of the vortex is always in the x direction. An examination of the form of the integral for the vector potential will convince the reader that it is somewhat bowl shaped, such that a plot of **A** versus radius will have a single maximum. The energy density will, of course, be found from the vector potential as

$$u=\frac{1}{8\pi}(E^2+B^2) \ . \tag{3.8}$$

While the electric field would be found as $\mathbf{E}=-\nabla\varphi-\partial\mathbf{A}/\partial t$, the first term does not contribute to an outgoing radiation field.

There will always be a radial node in the energy density. Where the **A** field peaks (at the rim of the bowl), both its derivative in y and its time derivative will cross through zero. The peak in **A** approximately corresponds to those points in space which are on the light cone with the annihilation of the pair. Thus, when one looks at the region of **A** which is out past the peak, one is seeing the region which is causally connected only with the infall; the region inside of the peak is causally connected with both the infall and the annihilation. If several simulations are done in which the initial separation is gradually decreased (decreasing the time of the approach), the outer peak will decrease in width and increase in height. This double-peaked structure is something that we did not predict from looking at the Φ Lagrangian, though it was observed in the ensuing simulations. It is clearly to be expected from consideration of the electromagnetic analogy.

The leading-order dependence of the B^2 term of the energy density on the angle can be found by rough calculation. Assume that the approach is taken along the x axis, with α as the angle from the axis. The magnetic field points in the z direction. With $D\equiv(t-t')^2-(\mathbf{x}-\mathbf{x}')^2$,

$$\mathbf{B}=B_z\hat{\mathbf{z}}=-\frac{\partial A_x}{\partial y}\hat{\mathbf{z}}\propto\int\frac{J(t')}{[D(t')]^{3/2}}\frac{\partial D(t')}{\partial y}dt'$$
$$\propto r\sin\alpha\int\frac{J(t')}{[D(t')]^{3/2}}dt' \ . \tag{3.9}$$

Thus the **B** field's leading-order contribution to the energy density is proportional to $\sin^2\alpha$.

E. The electromagnetic simulations

The dominant $\sin^2\alpha$ nature of the radiation field is unmistakable in both the Φ simulations and in the full electromagnetic calculations. In Fig. 10, we show the energy density arising from an electromagnetic source which is taken to be the vortex world line from a simple, head-on collision (see Fig. 1). When the radiated magnetic field is analyzed one finds that around 97% of the amplitude is proportional to $\sin\alpha$.

As mentioned above, we use the vortex world line as the source only until the particles are on the order of a

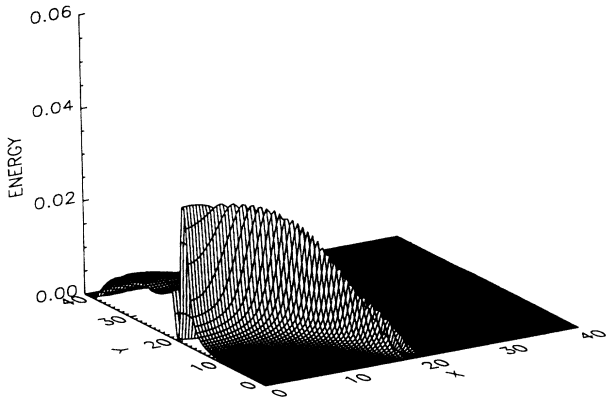

FIG. 10. Energy density at $t=40$, from electromagnetic analogy. Source taken from world line of simple head-on v-$\bar{v}$ collision; see Fig. 1(a) for corresponding Φ simulation plots

core radius apart, where we switch over to a source whose velocity falls linearly to zero. The height of the inner peak is a very sensitive function of the duration of time over which the deceleration takes place, with short times corresponding to high peaks. This inner peak is narrower than the peak observed in the Φ simulations. When the deceleration time is adjusted such that the height of the peaks are consistent, the electromagnetic simulation contains only about $\frac{2}{3}$ as much energy as the Φ simulation.

The location of the radial node also differs slightly between the two models. In the electromagnetic analogy, the node lies at a radius which sees the transition from the free fall to deceleration with a lightlike separation. If one extrapolates for the vortex world line in the Φ runs, it is found that the node is at a lightlike interval from the moment when the vortex and antivortex would have been directly over top of one another. These radii are close to each other, typically a distance of three spatial units from one another.

The electromagnetic analogy reproduces the angular dependence of the radiated field well. It reproduces the qualitative features of the radial dependence; we should expect no more than qualitative agreement here, considering that we have only an *ad hoc* method for mimicking the very energetic final moments of annihilation.

The disappearance of the particles releases large amounts of energy into the massive modes, as the magnitude of the field-changes dramatically at the annihilation point; in contrast, the electromagnetic analogy was derived assuming only massless Goldstone modes. We expect that the electromagnetic analogy could be put to good use in modeling radiation from an oscillating string or vortex-vortex scattering,[18] where there is less excitation of the massive modes.

From the point of view of numerical simulations there is no advantage in using the electromagnetic analogy over the original equations of motion. The number of degrees of freedom per site is small (two components of Φ and their conjugate momenta) and it is straightforward to simulate large systems.[19] We found the electromagnetic analogy most useful as a tool for qualitative understanding of annihilation patterns.

IV. CONCLUSIONS

We have identified several features in the radiation pattern from vortex-antivortex annihilation. The final annihilation emits a dipole radiation pattern, and linear acceleration during the approach radiates primarily transverse to the path as well. In collisions at nonzero impact parameter, additional energy is radiated at a tangent to the path, due to the circular component of acceleration. The fractional loss of energy from infall grows with increasing energy.

We have shown that the point-interaction analog to vortex dynamics, which is two-dimensional electrodynamics, reproduces the angular spectrum and much of the radial dependence of the radiation from vortex-antivortex annihilation, even though the derivation of the analogy is invalid when the pair is close. The electromagnetic analogy is not naturally capable of representing the final disappearance of the particles, and even our *ad hoc* method for mimicking the annihilation results in too little radiation during annihilation.

The electromagnetic analogy would be better applied to problems where much of the evolution occurs at a greater separation between the particles, perhaps as in the spiraling inward from large impact parameter of a vortex-antivortex pair. The measurements of radiation patterns which we have made are more easily done within the fundamental, Φ field. While the electromagnetic point-particle analog is useful for simple pencil and paper calculations, the results of the numerical simulations in this application do not justify the considerable effort of implementation.

It would be interesting to know if the radiation patterns we observe in our simulations could have astronomical consequences, either as part of the direct observation of a cosmic string, or as a contribution to galaxy formation. It seems more likely that one could observe these features in vortex annihilation in films of liquid crystals.

ACKNOWLEDGMENTS

We wish to thank Robert Brandenberger, Richard Davis, Roscoe Giles, Gerry Guralnik, Greg Kilcup, Eric Myers, Leandros Perivolaropoulos, Claudio Rebbi, and Paul Shellard for valuable conversations. This work was supported by the U.S. Department of Energy, and was carried out in part while the authors were visitors at Boston University (T.D. and M.H.) and Brown University (M.H.). We thank both those institutions for their hospitality.

APPENDIX

With the assumption that the vortices are separated by a distance larger than their core diameter, the interaction of two vortices may be considered to be that of a point, charged particle interacting with the electromagnetic field produced by the other source. The electromagnetic field tensor is related to the gradient of the phase of the Φ

field, and the coupling is proportional to the Φ field's vacuum expectation value. We present a derivation which is a simplified version of the one of Vilenkin and Vachaspati.[12] Another, similar derivation can be done starting from the Hamiltonian, and arriving at the same result via a canonical transformation.[13]

When the vortices are well separated, the magnitude of the field is nearly equal to its vacuum expectation value, and the approximation may be made that

$$\phi(x,t)=\rho(x,t)e^{i\theta(x,t)}\approx\eta e^{i\theta(x,t)} , \tag{A1}$$

$$L\approx\tfrac{1}{2}\eta^2\partial^\mu\theta\partial_\mu\theta . \tag{A2}$$

We consider the proposed equivalent electromagnetic Lagrangian. Working in the Gaussian system of units, this Lagrangian is

$$L_{\text{eff}}=-\frac{1}{16\pi}F_{\mu\nu}F^{\mu\nu}-J_\alpha A^\alpha , \tag{A3}$$

where

$$J_\alpha(x)=g\int V_\alpha(x')\delta^{(3)}(\mathbf{x}-\mathbf{x}')dx'_0 \tag{A4}$$

and

$$F^{\mu\nu}=\partial^\mu A^\nu-\partial^\nu A^\mu . \tag{A5}$$

The electromagnetic field tensor is related to its source by

$$\partial^\nu F_{\nu\mu}=4\pi J_\mu . \tag{A6}$$

Our problem is independent of the z spatial dimension, so the electromagnetic field tensor has only three nonzero components. These three components are relabeled in the more compact form

$$F_\mu=\tfrac{1}{2}\epsilon_{\mu\alpha\beta}F^{\alpha\beta} , \tag{A7}$$

where the greek indices run over 0,1,2. The components of the vector F are

$$F=(-B_z,+E_y,-E_x) . \tag{A8}$$

The equation of motion for F^μ is

$$\epsilon^{\alpha\beta\gamma}\partial_\beta F_\gamma=\tfrac{1}{2}\epsilon^{\alpha\beta\gamma}\epsilon_{\gamma\mu\nu}\partial_\beta F^{\mu\nu}=-4\pi J^\alpha . \tag{A9}$$

The gradient of a scalar is another quantity which has no curl, except for at a singular point. In the Φ field, the location of the vortex is singular, so we write

$$F_\mu=\bar{\eta}\partial_\mu\theta , \tag{A10}$$

where θ is the phase of the Φ field.

We relate $\bar{\eta}$ to the vacuum expectation value η by requiring that the stress tensors derived from the Φ and electromagnetic Lagrangians be identical. The symmetrized EM stress tensor is

$$\Theta^{\alpha\beta}=\frac{1}{4\pi}(g^{\alpha\mu}F_{\mu\lambda}F^{\lambda\beta}+\tfrac{1}{4}g^{\alpha\beta}F_{\mu\lambda}F^{\mu\lambda}) , \tag{A11}$$

or, in terms of $\bar{\eta}$ and θ,

$$\Theta^{\alpha\beta}=\frac{\bar{\eta}^2}{4\pi}(\partial^\beta\theta\partial^\alpha\theta-\tfrac{1}{2}g^{\alpha\beta}\partial^\mu\theta\partial_\mu\theta) . \tag{A12}$$

The stress tensor for the Goldstone-boson field is

$$T^{\alpha\beta}=\eta^2(\partial^\alpha\theta\partial^\beta\theta-\tfrac{1}{2}g^{\alpha\beta}\partial^\mu\theta\partial_\mu\theta) . \tag{A13}$$

Comparing the two stress tensors, it is seen that

$$\bar{\eta}=2\sqrt{\pi}\eta , \tag{A14}$$

which means that

$$F_\mu=\tfrac{1}{2}\epsilon_{\mu\alpha\beta}F^{\alpha\beta}=2\sqrt{\pi}\eta\partial_\mu\theta . \tag{A15}$$

The phase of the field must wind through 2π around a vortex. This additional constraint fixes the coupling in the effective Lagrangian. Using Stoke's theorem, we find that

$$\begin{aligned}2\pi=\oint_C dx^k d^k\theta&=(\bar{\eta})^{-1}\epsilon_{ij0}\int_S d\Sigma_{12}\partial_i F_j\\&=4\pi(\bar{\eta})^{-1}\int_S d\Sigma_{12}J^0\\&=4\pi(\bar{\eta})^{-1}g\int_S\int_{x'_0} d\Sigma_{12}dx'_0\delta^{(3)}(\mathbf{x}-\mathbf{x}') ,\end{aligned} \tag{A16}$$

where $d\Sigma_{12}$ is an element of surface area in the x-y plane. The coupling is proportional to the vacuum expectation value, as

$$g=\sqrt{\pi}\eta . \tag{A17}$$

[1]T. W. B. Kibble, J. Phys. A **9**, B87 (1976).

[2]A. Vilenkin, Phys. Rep. **121**, 263 (1985); N. Turok, Nucl. Phys. **B242**, 520 (1984); J. Ostriker, C. Thompson, and E. Witten, Phys. Lett. B **180**, 231 (1986).

[3]A. Vilenkin, Phys. Rev. Lett. **46**, 1169 (1981).

[4]R. Brandenberger, J. Phys. G **15**, 1 (1989).

[5]P. Shellard, Nucl. Phys. **B283**, 624 (1987).

[6]R. Matzner, Comput. Phys. **2**(5), 51 (1988).

[7]K. J. M. Moriarty, E. Myers, and C. Rebbi, Phys. Lett. B **207**, 411 (1988).

[8]A. Albrecht and N. Turok, Phys. Rev. Lett. **54**, 1868 (1985); Phys. Rev. D **40**, 973 (1989).

[9]D. Bennett and F. Bouchet, Phys. Rev. Lett. **60**, 257 (1988).

[10]T. DeGrand and R. Loft, Phys. Rev. B **35**, 8528 (1988).

[11]R. L. Davis and E. P. S. Shellard, Phys. Rev. Lett. **63**, 2021, (1989).

[12]A. Vilenkin and T. Vachaspati, Phys. Rev. D **35**, 1138 (1987).

[13]R. L. Davis and E. P. S. Shellard, Phys. Lett. B **214**, 219 (1988).

[14]E. Witten, Phys. Lett. **153B**, 243 (1985).

[15]R. L. Davis, Phys. Rev. D **32**, 3172 (1985).

[16]R. L. Davis and E. P. S. Shellard, Nucl. Phys. **B324**, 167 (1989).

[17]A. Dabholkar and J. M. Quashnock, Nucl. Phys. **B333**, 815 (1990).

[18]For vortex-vortex scattering in the gauge case, see P. J. Ru-

back, Nucl. Phys. **B296**, 669 (1988); E. P. S. Shellard and P. J. Ruback, Phys. Lett. B **209**, 262 (1988).

[19]We would like to note in passing that we also studied the X-Y limit of the model ($\lambda \to \infty, \eta = \text{const}$). In this limit the Higgs-boson mass ($m_H^2 \simeq \lambda \eta^2$) goes to infinity and the only low-energy modes in the system are Goldstone bosons and vortices. This system has only two degrees of freedom per site, θ, and its conjugate angular momentum L. Unfortunately a naive discretization of the equations of motion $\dot{\theta}_i = L_i$, $\dot{L}_i = \sum_{nn} \sin(\theta_i - \theta_{nn})$ has strong lattice artifacts: The vortex-antivortex pair can become pinned to lattice sites if the pair's initial orientation does not lie along a principal axis of the lattice. We do not know if this is a well-known phenomenon (it was not well known to us).